ROYAL SOCIETY OF CHEMISTRY

Check for updates

Mechanisms of CO oxidation on high entropy spinels†

Martina Fracchia, [ID] [ab] Paolo Ghigna, [ID] *[ab] Sara Stolfi,[ac]
Umberto Anselmi Tamburini,[ab] Mauro Coduri,[ab] Luca Braglia [ID] [cd] and
Piero Torelli[cd]

The CO oxidation reaction on $(Co,Mg,Mn,Ni,Zn)(Al,Co,Cr,Fe,Mn)_2O_4$ and $(Cr,Mn,Fe,Co,Ni)_3O_4$ high entropy spinel oxides was studied for what concerns its mechanism by means of *operando* soft X-ray absorption spectroscopy. In the $(Cr,Mn,Fe,Co,Ni)_3O_4$ high entropy spinel, CO oxidation starts at *ca.* 150 °C, and complete conversion to CO_2 is obtained at *ca.* 300 °C. For the $(Co,Mg,Mn,Ni,Zn)(Al,Co,Cr,Fe,Mn)_2O_4$ spinel oxides, in contrast, the reaction starts at *ca.* 200 °C, and complete conversion needs temperatures of the order of 350 °C. Concerning the reaction mechanism, we found that, in both cases, Mn is the active metal, *via* the Mn(II)/Mn(III) redox couple. CO is found to adsorb on surface Mn(III) sites and reduces them to Mn(II). The Mn(III) oxidation state is recovered by O_2, yielding CO_2. All the other transition metals are found to be inactive and act just as spectators. These findings are discussed in the framework of the present knowledge on high entropy oxides.

Introduction

Low-temperature CO oxidation is perhaps the most extensively studied reaction in the history of heterogeneous catalysis. The importance of this reaction resides in applications such as cleaning air and lowering internal combustion engine emissions.[1,2] As such, the catalytic oxidation of CO is employed in a variety of applications ranging from individual breathing air purifiers to submersible air compressor systems, when driven by diesel or petrol engines. An ideal catalyst for this reaction should therefore meet the conditions of low temperature activity and moisture stability. Platinum group metals are not poisoned by water, but their working temperature is usually above 100 °C.[1] Among noble metal catalysts, gold is water tolerant and highly active even at low temperatures, but it requires to be deposited in the form of nanoparticles on transition metal oxides.[3] In addition, water is considered a promoter for CO oxidation on gold.[4,5] The development of active and stable catalysts without noble metals for low-temperature CO oxidation under near ambient conditions remains a significant challenge. Under the trade name of

Hopcalite, a variety of manganese and copper spinels with different compositions are used at the moment in several devices for air purification from CO.[6] Hopcalite catalysts, however, are not particularly active at near-ambient temperatures and are also deactivated by the presence of moisture.[7] Among the metal oxides, the Co_3O_4 spinel is the most active for CO oxidation,[8] even below a temperature of –54 °C, but is severely deactivated by trace amounts of moisture (about 3–10 ppm) that are usually present in the feed gas.[9,10] In normal feed gas, most of the active sites of Co_3O_4 are covered by H_2O, so the adsorption of CO and oxygen is appreciably hindered.[11] Significant increases in the CO adsorption strength in the presence of water were recently proposed as an additional source of deactivation.[12]

The mechanism of the reaction involves reactive CO adsorption on the surface Co(III) cation with the formation of Co(II),[13–16] and oxidation of the adsorbed CO by surface oxygen coordinated with three Co(II).

In the quest for new catalysts for CO oxidation, the prototypical high entropy oxide (HEO) $Mg_{0.2}Co_{0.2}Ni_{0.2}Cu_{0.2}Zn_{0.2}O$, bearing the rock-salt structure, has been recently found to be active in the reaction at quite low temperature.[17] In HEOs, it was initially proposed that configurational entropy leads to the stabilization of a single-phase crystal structure in multicomponent (five or more) systems, compensating for unfavorable enthalpy contributions.[18,19] Although this rationale has been recently questioned,[20–22] the interest in HEOs is still growing, due to the potential of obtaining novel properties by exploiting the enormous number of possible elemental combinations, the

[a] *Dipartimento di Chimica, Università di Pavia, V.le Taramelli 13, I-27100, Pavia, Italy. E-mail: paolo.ghigna@unipv.it*

[b] *INSTM, Consorzio Interuniversitario per la Scienza e Tecnologia dei Materiali, Via Giusti 9, 50121, Firenze, Italy*

[c] *CNR-Istituto Officina dei Materiali, TASC, Trieste, Italy*

[d] *Area Science Park, Trieste, Italy*

† Electronic supplementary information (ESI) available. See DOI: https://doi.org/10.1039/d4cp04359f

facile synthesis, and the possibility of exploiting several synthetic routes for obtaining highly reproducible materials. Over the last few years, HEOs have been synthesized in a wide variety of crystal structures other than the rock salt, such as spinels,[23–25] fluorite,[26–28] perovskites,[29,30] and many more.[31–33]

Recently, we investigated the mechanisms of the CO oxidation reaction on the $Mg_{0.2}Co_{0.2}Ni_{0.2}Cu_{0.2}Zn_{0.2}O$ HEO, by means of *operando* soft X-ray absorption spectroscopy (Soft-XAS) experiments at the transition metal (TM) $L_{2,3}$-edges.[34,35] Briefly, the main results of our investigation are: (i) Cu is the only active metal, and all the other TMs do not participate in the catalytic cycle; (ii) the reaction proceeds *via* reactive adsorption of CO on surface Cu(II) sites to give Cu(I); (iii) Cu(II) is restored by external oxygen, thus desorbing CO_2 from the surface; (iv) the role of configurational entropy is likely to stabilize the Cu(II) oxidation state, that is easily and irreversibly reduced to Cu(I) in pure CuO, thus preventing the catalytic cycle to take place on this last simple oxide.

Spinel oxides have been largely employed as catalysts for the CO oxidation. As a matter of fact, a number of recent studies have investigated the catalytic activity of various spinel catalysts for CO oxidation, with the most promising results observed in manganese-containing catalysts in combination with other metals such as copper and cobalt. In $CuMn_2O_4$[36] and $CuMn_2O_2$,[37] manganese plays a critical role in forming the active species Mn^{3+} and Mn^{4+}, facilitating a redox cycle that enhances oxygen transfer and improves the material ability to oxidize CO at low temperatures. The synergy between copper and manganese generates effective catalytic centers that are strongly dependent on the Cu/Mn molar ratio.[38]

Furthermore, $MnCo_2O_4$ exhibits high activity for CO oxidation at moderate temperatures (30–300 °C) due to its substantial surface area and the interaction between manganese and cobalt.[39] Additionally, among the series of catalysts $Mn_5Co_1O_x$ synthesized by Bulavchenko *et al.*,[40] the one calcined at 400 °C demonstrates the best catalytic performance, primarily attributed to a high surface concentration of Mn^{4+} species.

Therefore, manganese (Mn) plays a crucial role in enhancing catalytic activity, particularly in comparison to spinel materials lacking manganese. For instance, $(Mn_{0.11}Co_{0.89})(Co_{1.03}Mn_{0.97})O_4$, developed by Hudy *et al.*,[41] shows significantly higher surface areas and smaller crystal sizes compared to other spinels like pure Co_3O_4, which is directly correlated with improved catalytic performance for CO oxidation. Specifically, Mn–Co samples exhibit better selectivity for CO adsorption and conversion due to their increased oxygen mobility and optimal electronic band structures.

Based on the above, we aim in this paper to extend our investigation to the $(Cr,Mn,Fe,Co,Ni)_3O_4$ (hereby referred to as S5) and $(Co,Mg,Mn,Ni,Zn)(Al,Co,Cr,Fe,Mn)_2O_4$ (here referred to as S8) high entropy spinels that we found to be active in the CO oxidation reaction, also using *operando* Soft-XAS experiments at the transition metal (TM) $L_{2,3}$-edges. We take advantage of the fact that, compared to XAS in the hard X-ray regime, Soft-XAS in the total electron yield (TEY) mode combines two unique features, *i.e.* the capability of directly monitoring the density of empty 3d states for TMs and (ii) the surface sensitivity,

which, due to the low value of electron escape depth, limits the thickness of the probed sample to few atomic layers below the surface.[42–45] This approach allows answering the main questions concerning the reaction mechanisms of TM-based heterogeneous catalysts, namely the local electronic structure of the transition metals, their oxidation states, the nature of the active surface site, and possible changes of all these properties thereof during the reaction course. As a final point, we note here that XAS is element selective, and this allows coping with the chemical complexity of these systems.

Results and discussion

Metal oxidation state, cation distribution, and total configurational entropy for the spinels

The K-edge XAS spectra of TMs provide direct information on the oxidation state of the metals and their cation distribution on the tetrahedral and octahedral sites of the spinel structure. We point out that this is bulk information, as the penetration depth of X-rays in this energy range is of the order of few microns. In principle, the edge energy position can be fitted against standards to yield a precise value for the oxidation state. However, this is made difficult in the current case, due to the presence of two cationic sites that make the spectral shape of the edge quite complicated.

Therefore, we here refer to the methods used in our previous paper in the case of $(Co,Mg,Mn,Ni,Zn)(Al,Co,Cr,Fe,Mn)_2O_4$, for which we found the cation distribution corresponding to the formula $(Mg_{0.2}Mn_{0.2}Zn_{0.2}Fe_{0.1}Co_{0.3})^T(Al_{0.2}Cr_{0.2}Mn_{0.2}Fe_{0.15}Co_{0.15}Ni_{0.1})_2^OO_4$,[23] where the superscripts T and O refer to the tetrahedral and octahedral sites, respectively. The K-edge spectra of the two spinels are reported in Fig. 1. Briefly, this method consists of the simultaneous comparison of the spectral shape of the XANES and the intensity of the pre-edge peaks at different metal K-edges with those of selected standards.

Concerning the oxidation state of TMs, we found that Cr is in the Cr(III) oxidation state, Mn is in the mixed Mn(II) + Mn(III) oxidation state, Fe is in the mixed Fe(II) + Fe(III) oxidation state, Co is in the mixed Co(II) + Co(III) oxidation state, and Ni is in the Ni(II) oxidation state. Following the same procedure for the $(Cr,Mn,Fe,Co,Ni)_3O_4$ spinel, we found that Cr is in the Cr(III)

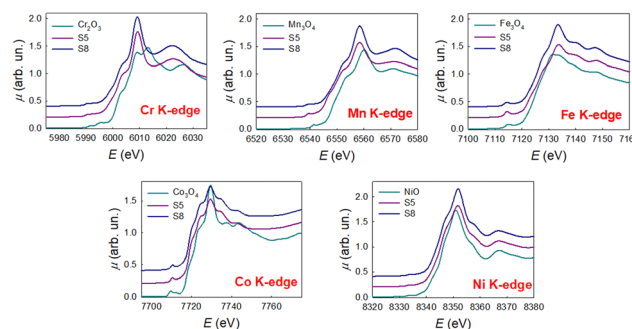**Fig. 1** Cr, Mn, Fe, Co and Ni K-edge XAS spectra of the S5 and S8 high entropy spinels at RT. The spectra of Cr_2O_3, Mn_3O_4, Fe_3O_4, Co_3O_4 and NiO are also shown for references of the oxidation state.

This journal is © the Owner Societies 2025

Phys. Chem. Chem. Phys., 2025, **27**, 3412–3419 | **3413**

oxidation state and in the octahedral sites, Mn is in the mixed Mn(II) + Mn(III) oxidation state and both in tetrahedral and octahedral sites, Fe is in the mixed Fe(II) + Fe(III) oxidation state and both in tetrahedral and octahedral sites, Co is in the mixed Co(II) + Co(III) oxidation state and both in tetrahedral and octahedral sites, and Ni is in the Ni(II) oxidation state and only in the octahedral sites.

We then have the formula $(Mn_{0.2}Fe_{0.4}Co_{0.4})^T(Cr_{0.3}Mn_{0.2}Fe_{0.1}Co_{0.1}Ni_{0.3})_2^OO_4$. Using the equation $S_{config} = -R\left(\sum_{i,T}\chi_i\ln\chi_i + 2\sum_{i,O}\chi_i\ln\chi_i\right)$ for the configurational entropy, we have $S_{config} = 5.9R$ and $S_{config} = 4.5R$, for the two spinels, respectively. Remarkably, the two spinels have a similar cation distribution for what concerns the transition metals: the only remarkable differences concern Mn, which is slightly more oxidized in S8 than in S5, and Fe, which, according to the pre-edge peak intensity, shows a more pronounced occupation of tetrahedral sites in S5 than in S8.

These conclusions are supported also by the $L_{2,3}$-edge spectra reported in Fig. 2.

We here remind that the $L_{3,2}$-edge spectra of 3d transition metals are dominated by large peaks due to electronic transitions from 2p to the empty valence 3d states, transitions to the 4s states being in principle of negligible intensity. Due to the localized character of both 2p and 3d orbitals in the 3d metals, these transitions can be treated as quasi-atomic in nature, and, therefore, can be used for a truthful assessment of oxidation states and local coordination. Another point to note is the fact that the localised nature of the 3d states and the strong overlap between 2p and 3d states allow a simple treatment of these transition in terms of multiplet calculations.[45]

For both spinels, the spectra at RT present remarkable similarities, confirming that both the mean oxidation state and the cation distribution are very similar. In Fig. 2, the spectra of Cr_2O_3, Mn_3O_4, Fe_3O_4, Co_3O_4, and NiO are also shown for better reference of the oxidation state. It should be noted that Mn_3O_4, Fe_3O_4, and Co_3O_4 are normal spinels, with the transition metals in both tetrahedral and octahedral sites. Cr_2O_3 has a corundum structure, with Cr in a slightly distorted octahedral environment, and NiO has a rock-salt structure, with Ni in a regular octahedral coordination. The comparison of the spectra of the S8 and S5 spinels with the corresponding standards, therefore, confirms the assignation of the cation distribution and oxidation state, with the possible exception of Co, for which the spectra at the Co $L_{2,3}$-edges are remarkably different with respect to that of Co_3O_4. However, this disagreement can be explained by taking into account that the cation distribution for Co in S8 and S5 significantly differs from what is expected for a normal spinel, both having a significant amount of Co in the tetrahedral sites. Indeed, it can be shown that Co(III) in the tetrahedral sites gives sizable spectral intensity in the region around 777 eV.[46] This is confirmed by multiplet calculations as reported in Fig. S1 (see the ESI†).

Mechanism of CO oxidation

The determination of the mechanisms of CO oxidation over the high entropy spinels implies the determination of the active metal(s), their oxidation states, and possible changes thereof during the course of the reaction. To this aim, and taking advantage of the atomic selectivity of XAS, we performed the *operando* experiment at the transition metal $L_{2,3}$-edges at 250 °C and under two different atmospheres: the stoichiometric CO + 1/2O₂ gas mixture and then pure O₂ for re-oxidising possible reduced species (see the Experimental section for further details). We decided to conduct the mechanistic experiment at 250 °C as at this temperature the two spinels show a remarkable difference in their catalytic activity, as detailed below.

In addition, we here remark that, compared to K-edge XAS, transition metal $L_{2,3}$-edge XAS directly probes the metal valence states, as the 2p → 3d transitions are directly accessible *via* dipolar transitions observing the $\Delta\ell = \pm 1$ selection rule. Moreover, in the TEY detection mode, the technique is surface sensitive and, therefore, is an election probe for the identification of the oxidation states of transition metals at the surface, and possible modifications thereof.

Fig. 3 displays the Cr, Fe, Co and Ni $L_{2,3}$-edge XAS spectra of S8 and S5 under the two different atmospheres: note that in the stoichiometric CO + 1/2O₂ gas mixture, and at 250 °C, both spinels are active in the CO oxidation reaction (see the ESI† for additional details). It is well evident that no changes are detected for all four transition metals; therefore, we conclude that the active sites for the catalytic reaction do not involve Cr, Fe, Co, or Ni.

Fig. 4 shows the CO oxidation activity of the S5 and S8 spinels, determined as explained in the Experimental section. It is quite apparent that the S5 spinel is more active than S8: on the S5 spinel, the CO conversion starts to be noticeable at *ca.* 150°, while complete conversion is obtained at *ca.* 300 °C. For S8, a reasonable conversion is obtained only at 200 °C, while complete conversion is reached at 350 °C. We also observe that at 250 °C the two spinels show a remarkable difference in the catalytic activity, and this explain our choice to conduct the mechanistic experiments at this temperature. In Fig. 4, therefore, the Mn $L_{2,3}$-edge XAS spectra of the S8 and S5 spinels at RT and 200 °C in He, at 250 °C in the stoichiometric CO + 1/2O₂ gas mixture, and then at
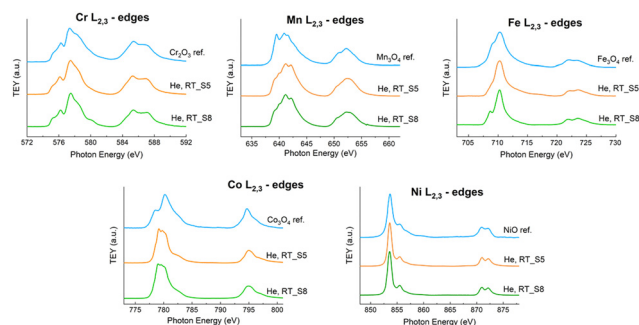

Fig. 2 Cr, Mn, Fe, Co and Ni $L_{2,3}$-edge XAS spectra of the S5 and S8 high entropy spinels at RT. The spectra of Cr_2O_3, Mn_3O_4, Fe_3O_4, Co_3O_4 and NiO are also shown for references of the oxidation state.
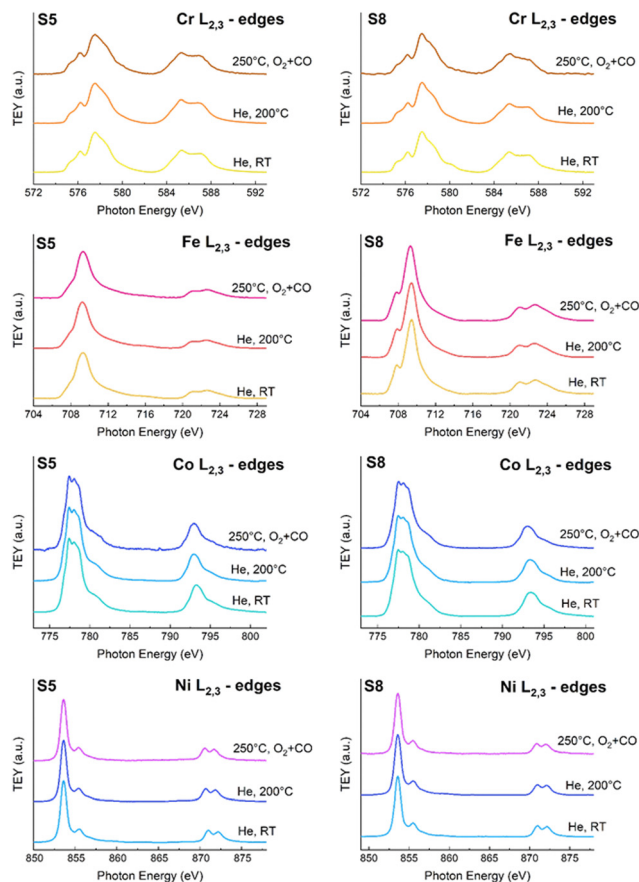
3414 | *Phys. Chem. Chem. Phys.*, 2025, **27**, 3412–3419

This journal is © the Owner Societies 2025

Fig. 3 *Operando* Cr, Fe, Co and Ni $L_{2,3}$-edge XAS spectra of the S8 and S5 HEO materials.

Fig. 4 CO oxidation activity and *operando* Mn $L_{2,3}$-edge XAS spectra of the S8 and S5 HEO materials: the energy region between 638.5 and 640.5 eV is shown on an enlarged energy scale for better evidencing the peak of Mn(II).

220 °C in O_2, are shown. When heating the samples in He at *ca.* 200 °C, a marked increase in the intensity of the peak at *ca.* 639.2 eV is detected in both cases. This peak is assigned to Mn(II) on the basis of literature data and multiplet calculations (see the ESI† for additional details). Therefore, this increase in intensity can be attributed to a partial reduction of Mn(III) to Mn(II). This reduction, in turn, may be attributed to the removal of adsorbed surface oxygen species near Mn, creating surface oxygen deficient Mn surface sites.

For the S8 spinel, in the stoichiometric CO + $1/2O_2$ gas mixture at 250 °C, this increase is largely more pronounced, while the peak amplitude can be reduced by stopping the CO flow and flowing only oxygen on the sample. These results show unequivocally that the CO oxidation on the S8 HEO spinel involves the reactive adsorption of CO on the Mn(III) sites at the surface, causing a charge transfer from CO to Mn, thus leading to Mn(II). Then, the adsorbed CO is oxidised by oxygen to give CO_2 reoxidizing Mn(II) to Mn(III).

For the S5 spinel, the results are rather similar, but the intensity of the Mn(II) peak at *ca.* 639.2 eV is slightly decreased in the stoichiometric CO + $1/2O_2$ mixture at 250 °C, and the reduction in amplitude by flowing pure oxygen at 220 °C is also less pronounced. In addition, a marked increase in the intensity of the Mn(II) peak is detected in heating in pure oxygen at 250 °C: we do not have a definitive explanation for this, but we
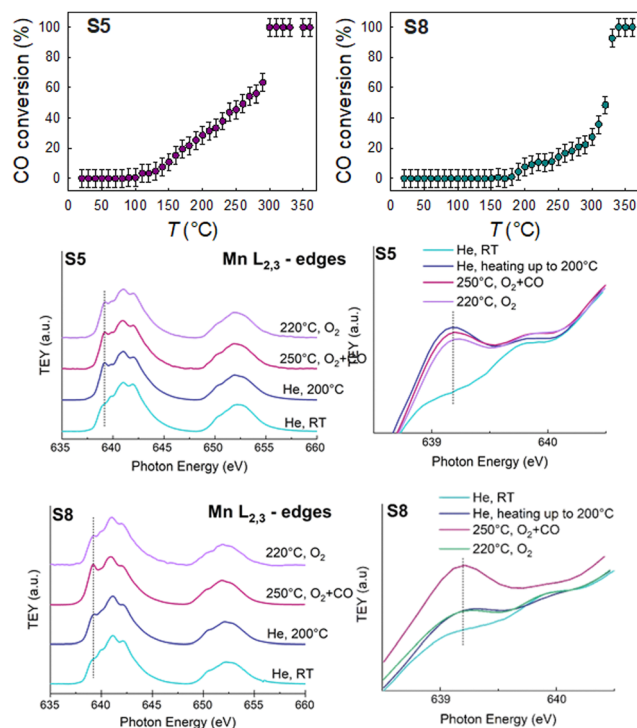
can suggest that it may be due to the desorption of some hydroxyl species and to the formation of defective surface sites.

Despite the fact that there are some differences in the behavior between the S5 and S8 spinels, it remains certain that on both materials CO oxidation proceeds *via* reactive adsorption of CO on surface Mn(III) sites to produce Mn(II)–CO adsorbates, which are then re-oxidized to Mn(III) by oxygen, yielding CO_2. The catalytic cycle is outlined in Fig. 5A.

Although a full catalytic characterization on these systems is well beyond the aims of this work, we point out that additional information on the activity towards the CO oxidation reaction by the S5 and S8 spinels can be obtained by analysing the gas composition downstream of the *operando* Soft-XAS cell. This can be done as a micro-GC is placed on the exhaust gas pipeline (see the Experimental section). In Fig. 5B, the ratio of the integrated areas of the GCI peaks of CO_2 and CO + O_2 are plotted *vs.* time for the two spinels. It is quite apparent that, at 250 °C, the S5 spinel is more active than S8, confirming the data in Fig. 4. Several factors can add in this case to explain the different phenomenology: differences in the rate of reaction between reduction and oxidation on the two spinels, the presence of multiple adsorption sites on the surface, the difference in the surface area between the two spinels, *etc.* The width of the peaks in the diffraction patterns in Fig. 5C points towards a grain dimension in the μm range in both cases, suggesting that the differences in the surface area are not relevant in this case. Indeed, the two samples have very similar values of the surface
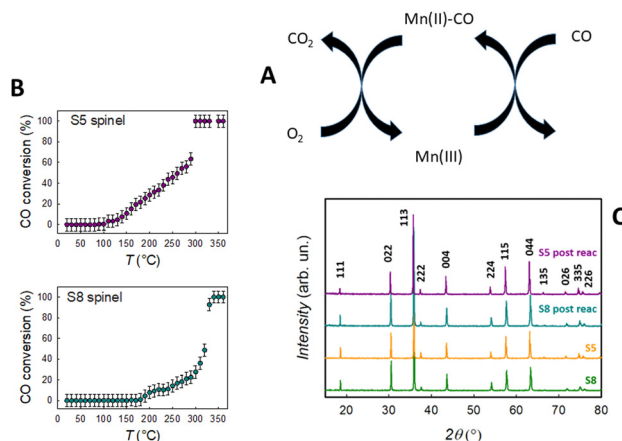
This journal is © the Owner Societies 2025

Phys. Chem. Chem. Phys., 2025, **27**, 3412–3419 | **3415**

Fig. 5 (A) Scheme of the catalytic cycle involving the Mn(II)/Mn(III) redox couple on the S5 and S8 high entropy spinels. (B) Comparison of the activity of the S5 and S8 spinels. The graph shows the time evolution of the ratio of the integrated area of the CG peaks of CO_2 and $CO + O_2$ over the two spinels. (C) X-ray powder diffraction patterns of the S5 and S8 spinels as prepared (yellow and green curves) and after (cyan and purple curves) the catalytic reaction.

area, as determined by BET: for S5 and S8, we found 1.40 ± 0.01 m² g⁻¹ and 1.70 ± 0.01 m² g⁻¹, respectively.

We can note as a general remark that the activity of a catalyst is the result of a fine balance in the terms that concur to the stabilization of the surface active sites and the absorbed species on the surface. This is schematized by the Sabatier principle: the strength of adsorption should be neither too strong nor too weak. In this respect, we note that configurational entropy is high for both spinels, and in both cases, it acts as the stabilizing term.

This is also demonstrated by the powder diffraction patterns shown in Fig. 5C, showing that the spinel structure is stable during the course of the reaction. However, configurational entropy is much higher for the S8 spinel than for the S5: it could be concluded that the Mn(II)/Mn(III) redox couple is stabilized by configurational entropy in both cases, but, for S8, this stabilization is too large.

Experimental

Synthetic procedures

Crystalline $(Cr,Mn,Fe,Co,Ni)_3O_4$ and $(Co,Mg,Mn,Ni,Zn)(Al, Co,Cr,Fe,Mn)_2O_4$ were prepared by a sol–gel approach starting from the corresponding metal nitrates, mixed in the stoichiometric amounts and dissolved in water together with an excess of citric acid. The as-prepared solution was heated overnight at 80 °C under stirring, and the obtained gel was heated in an oven at 120 °C and finally calcined at 1000 °C for 12 h. All the starting reagents were purchased at an analytical grade from Sigma-Aldrich and were used without further purification.

Material characterization

Both samples was first checked for phase purity by X-ray diffraction (XRD) using a D8 Advance diffractometer (Bruker) with Cu Kα radiation. The chemical homogeneity at the atomic

level was proved by scanning electron microscopy (SEM) and energy dispersive X-ray spectroscopy (EDS) for the S8 spinel, using a Tescan Mira3XMU microscope operating at 20 kV and equipped with an EDAX EDS analysis system. See ref. 23, for additional details. The cation distribution and inversion degree of the two spinel materials were determined by means of X-ray absorption spectroscopy (XAS) at the Cr, Mn, Fe, Co, Ni, and Zn K-edges. All the measurements were made at the XAFS beamline of the ELETTRA synchrotron radiation facility. The spectra were acquired at room temperature in transmission mode. For the measurement, an appropriate amount of powder, weighted to give an edge jump close to 1 in logarithmic unit, was thoroughly mixed with cellulose in an agate mortar and pestle, and then pressed to pellets. The ring current and energy were 200 mA and 2.4 GeV, respectively. A Si(111) double-crystal monochromator was used ensuring high-order harmonic rejection by detuning the second crystal. A water-cooled, Pt-coated silicon mirror was used to obtain vertical collimation of the beam. The spectra were aligned in energy using a reference metal foil for energy calibration and measured simultaneously with the sample. For the XANES analysis, the spectra were first pre-edge subtracted after fitting the pre-edge region with a straight line, and then normalized to unit absorption at 400 eV after the edge, where the EXAFS oscillations are not visible anymore. The procedure was performed using the Athena code.[47] For the $(Co,Mg,Mn,Ni,Zn)(Al,Co,Cr,Fe,Mn)_2O_4$ spinel, the results have been already reported.[23]

Catalytic tests

Catalytic tests were performed by means of a tubular quartz reactor. *ca.* 5 mg of each of the spinels were loaded in the middle of the reaction tube and held in place by means of quartz wool. The reactor was then placed in a tubular furnace, and was feed by a stoichiometric $CO + O_2$ mixture. The CO_2 concentration in the exhaust pipeline of the reactor was measured by means of a non-dispersive infrared CO_2 sensor (gravity, Dfrobot SEN0219). The sensor was completely embedded in the gas flowing out of the reactor, and its response was converted in CO_2 concentrations by means of a National Instrument data acquisition interface, after calibration with a standard (Linde, 99.999%). The BET specific surface area (SSA) of the materials was measured by N_2 adsorption/desorption at liquid nitrogen temperature using a Micromeritics Tristar II 3020 V1.03 apparatus, after out-gassing at 300 °C for 1 h under N_2 stream.

Soft-XAS experiment

For the Soft-XAS experiment, a small amount of the spinel materials (5 mg *ca.*), in form of loose powder, was hand pressed on the sample holder of the reaction cell of the APE beamline at the ELETTRA synchrotron radiation facility. All the measurements were performed keeping the sample grounded through the picoammeter and applying a positive bias voltage of 40 V to the membrane. The cell is mounted in the UHV chamber of the APE-HE beamline, coaxially with the X-ray beam. The experiment was performed following the same procedure explained elsewhere.[34] The measurements were performed at the Cr, Mn,

3416 | *Phys. Chem. Chem. Phys.*, 2025, **27**, 3412–3419

This journal is © the Owner Societies 2025

Fe, Co, and Ni $L_{2,3}$-edges. Surface sensitivity is obtained by collecting the XAS spectra in total electron yield mode: the estimated probed depth is *ca.* 3–4 nm.[44] To ensure for maximum gas purity, especially concerning water and carbon oxides, the He carrier gas was passed through a liquid N_2 trap before entering the cell. The spectra at all the edges have been background subtracted by fitting the pre-edge with a straight line, and then normalised to unit absorption after the L_3 edge. The experiments were conducted in flowing He (50 standard cubic centimeter per minute, SCCM), either pure or with the addition of CO (2 SCCM), O_2 (2 SCCM), or with the stoichiometric CO + O_2 mixture (2 + 1 SCCM, respectively). All gases were supplied by Linde, with a purity of at least 99.999%. The CO_2 concentration in the exhaust pipeline of the APE *operando* cell was measured by means of an Agilent 490 Micro Gas Chromatography System, equipped with two chromatographic columns connected to the cell gas-line output: the first column is a volamine, heated to 110 °C. It uses He as a carrier gas, enabling the detection of CO_2 and CO; the second column is a molecular sieve, heated to 40 °C, with N_2 as a carrier gas, and it was not used in this experiment.

Conclusions

The mechanisms of the CO oxidation reaction over the (Cr,Mn,Fe,-Co,Ni)$_3$O$_4$ (S5) and (Co,Mg,Mn,Ni,Zn)(Al,Co,Cr,Fe,Mn)$_2$O$_4$ (S8) high entropy spinels have been investigated by means of *operando* soft X-ray absorption spectroscopy, extending our previous investigation.[33] In both cases, we found that the reaction proceeds *via* the Mn(II)/Mn(III) redox couple, according to the catalytic cycle shown in Fig. 5a. All the other transition metals are inactive and act as spectators. Given the chemical complexity of the two spinels, the atomic selectivity of X-ray absorption spectroscopy is a crucial factor for allowing mechanistic investigations.

The S5 spinel is more active than the S8 spinel, and this result can be explained by the fact that the stabilizing configurational entropy term is higher for S8 than for S5. This is an important result in the framework of the science of high entropy oxides, as these materials are often studied for applications concerning catalysis or as materials for lithium batteries. As a general conclusion, we can here remark that all these applications require a certain degree of reactivity of the involved material, and configurational entropy is always a stabilizing term, lowering the reactivity; in other terms, in the search for reactivity, adding stability is not always a good quest.

Author contributions

The manuscript was written through contributions of all authors. All authors have given approval to the final version of the manuscript.

Data availability

The data supporting this article have been included as part of the ESI.†

Conflicts of interest

There are no conflicts to declare.

Acknowledgements

Notes and references

1 M. Shelef and R. W. McCabe, Twenty-five years after introduction of automotive catalysts: what next?, *Catal. Today*, 2000, **62**(1), 35–50, DOI: **10.1016/S0920-5861(00)00407-7**.

2 N. K. Soliman, Factors affecting CO oxidation reaction over nanosized materials: A review., *J. Mater. Res. Technol.*, 2019, **8**, 2395–2407, DOI: **10.1016/j.jmrt.2018.12.012**.

3 M. Daté, M. Okumura, S. Tsubota and M. Haruta, Vital Role of Moisture in the Catalytic Activity of Supported Gold Nanoparticles, *Angew. Chem., Int. Ed.*, 2004, **43**(16), 2129–2132, DOI: **10.1002/anie.200453796**.

4 T.-M. Tran-Thuy, T.-L. Yu and S. D. Lin, How H_2O may influence ambient CO oxidation over Au/BN, *Appl. Catal., B*, 2022, **314**, 121492, DOI: **10.1016/j.apcatb.2022.121492**.

5 T.-M. Tran-Thuy, C.-C. Chen and S. D. Lin, Spectroscopic Studies of How Moisture Enhances CO Oxidation over Au/BN at Ambient Temperature, *ACS Catal.*, 2017, **7**(7), 4304–4312, DOI: **10.1021/acscatal.7b01374**.

6 J. P. N. Kembo, J. Wang, N. Luo, F. Gao, H. Yi, S. Zhao, Y. Zhou and X. Tang, A review of catalytic oxidation of carbon monoxide over different catalysts with an emphasis on hopcalite catalysts, *New J. Chem.*, 2023, **47**, 20222–20247, DOI: **10.1039/D3NJ03074A**.

7 C. Yoon and D. L. Cocke, The design and preparation of planar models of oxidation catalysts. I. Hopcalite, *J. Catal.*, 1988, **113**(2), 267–280, DOI: **10.1016/0021-9517(88)90256-4**.

8 Y. F. Y. Yao, The oxidation of hydrocarbons and CO over metal oxides. III. Co$_3$O$_4$, *J. Catal.*, 1974, **33**(1), 108–122, DOI: **10.1016/0021-9517(74)90250-4**.

9 F. Grillo, M. M. Natile and A. Glisenti, Low temperature oxidation of carbon monoxide: The influence of water and oxygen on the reactivity of a Co$_3$O$_4$ powder surface, *Appl.*

This journal is © the Owner Societies 2025

Phys. Chem. Chem. Phys., 2025, **27**, 3412–3419 | **3417**

Catal., B, 2004, **48**(4), 267–274, DOI: **10.1016/j.apcatb.2003.11.003**.

10 J. Bae, V. Shin, H. Jeong, B.-S. Kim, J. W. Han and H. Lee, Highly Water-Resistant La-doped Co_3O_4 catalyst for CO Oxidation, *ACS Catal.*, 2019, **9**(11), 10093–10100, DOI: **10.1021/acscatal.9b02920**.

11 N. Yigit, A. Genest, S. Terloev, J. Möller and G. Rupprechter, Active sites and deactivation of room temperature CO oxidation on Co_3O_4 catalysts: combined experimental and computational investigations, *J. Phys.: Condens. Matter*, 2022, **34**(35), 354001, DOI: **10.1088/1361-648X/ac718b**.

12 G. Fickenscher, C. Hohner, T. Xu and J. Libuda, Adsorption of D_2O and CO on $Co_3O_4(111)$: Water Stabilizes Coadsorbed CO, *J. Phys. Chem. C*, 2011, **125**(48), 26785–26792, DOI: **10.1021/acs.jpcc.1c07393**.

13 P. Broqvist, I. Panas and H. Persson, A DFT study on CO oxidation over Co_3O_4, *J. Catal.*, 2002, **210**(1), 198–206, DOI: **10.1006/jcat.2002.3678**.

14 J. Jansson, Low-temperature CO oxidation over Co_3O_4/Al_2O_3, *J. Catal.*, 2000, **194**(1), 55–60, DOI: **10.1006/jcat.2000.2924**.

15 L. Lukashuk, N. Yigit, R. Rameshan, E. Kolar, D. Teschner, M. Hävecker and G. Rupprechter, *Operando* Insights into CO Oxidation on Cobalt Oxide Catalysts by NAP-XPS, FTIR, and XRD, *ACS Catal.*, 2018, **8**(9), 8630–8641, DOI: **10.1021/acscatal.8b01237**.

16 S. A. Singh and G. Madras, Detailed mechanism and kinetic study of CO oxidation on cobalt oxide surfaces, *Appl. Catal., A*, 2015, **504**, 463–475, DOI: **10.1016/j.apcata.2014.10.024**.

17 H. Chen, J. Fu, P. Zhang, H. Peng, C. W. Abney, K. Jie, X. Liu, M. Chi and S. Dai, Entropy-stabilized metal oxide solid solutions as CO oxidation catalysts with high-temperature stability, *J. Mater. Chem. A*, 2018, **6**(24), 11129–11133, DOI: **10.1039/c8ta01772g**.

18 C. W. Rost, E. Sachet, T. Borman, A. Moballegh, E. C. Dickey, D. Hou, J. L. Jones, S. Curtarolo and J.-P. Maria, Entropy-stabilized oxides, *Nat. Commun.*, 2015, **6**(1), 1–8, DOI: **10.1038/ncomms9485**.

19 A. Sarkar, Q. Wang, Q. Schiele, M. R. Chellali, S. S. Bhattacharya, V. Wang, T. Brezesinski, V. Hahn, L. Velasco and B. Breitung, High-Entropy Oxides: Fundamental Aspects and Electrochemical Properties, *Adv. Mater.*, 2019, **31**(26), 1806236, DOI: **10.1002/adma.201806236**.

20 M. Fracchia, M. Coduri, M. Manzoli, P. Ghigna and U. Anselmi-Tamburini, Is configurational entropy the main stabilizing term in rock-salt $Mg_{0.2}Co_{0.2}Ni_{0.2}Cu_{0.2}Zn_{0.2}O$ high entropy oxide?, *Nat. Commun.*, 2022, **13**(1), 1–4, DOI: **10.1038/s41467-022-30674-0**.

21 S. S. Aamlid, M. Oudah, J. Rottler and A. M. Hallas, Understanding the Role of Entropy in High Entropy Oxides, *J. Am. Chem. Soc.*, 2023, **145**(11), 5991–6006, DOI: **10.1021/jacs.2c11608**.

22 M. Fracchia, M. Coduri, P. Ghigna and U. Anselmi-Tamburini, Phase stability of high entropy oxides: A critical review, *J. Eur. Ceram. Soc.*, 2023, **44**(2), 585–594, DOI: **10.1016/j.jeurceramsoc.2023.09.056**.

23 M. Fracchia, M. Manzoli, U. Anselmi-Tamburini and P. Ghigna, A new eight-cation inverse high entropy spinel with large configurational entropy in both tetrahedral and octahedral sites: Synthesis and cation distribution by X-ray absorption spectroscopy, *Scr. Mater.*, 2020, **188**, 26–31, DOI: **10.1016/j.scriptamat.2020.07.002**.

24 J. Dąbrowa, M. Stygar, A. Mikuła, A. Knapik, K. Mroczka, W. Tejchman, M. Danielewski and M. Martin, Synthesis and microstructure of the $(Co,Cr,Fe,Mn,Ni)_3O_4$ high entropy oxide characterized by spinel structure, *Mater. Lett.*, 2018, **216**, 32–36, DOI: **10.1016/j.matlet.2017.12.148**.

25 M. Coduri, M. Fracchia, M. Guerrini, M. Dejoie, P. Ghigna and U. Anselmi-Tamburini, Novel In-based high entropy spinel oxides with tunable lattice parameter, *J. Eur. Ceram. Soc.*, 2023, **43**(7), 2728–2739, DOI: **10.1016/j.jeurceramsoc.2022.12.047**.

26 J. Gild, M. Samiee, J. L. Braun, T. Harrington, T. Vega, P. E. Hopkins, P. E. Vecchio and J. Luo, High-entropy fluorite oxides, *J. Eur. Ceram. Soc.*, 2018, **38**(10), 3578–3584, DOI: **10.1016/j.jeurceramsoc.2018.04.010**.

27 J.-P. Wright, Q. Wang, Q. Huang, A. Nieto, A. Chen and J. Luo, From high-entropy ceramics to compositionally-complex ceramics: A case study of fluorite oxides, *J. Eur. Ceram. Soc.*, 2020, **40**(5), 2120–2129, DOI: **10.1016/j.jeurceramsoc.2020.01.015**.

28 L. Spiridigliozzi, C. Ferone, C. Cioffi and G. Dell'Agli, A simple and effective predictor to design novel fluorite-structured High Entropy Oxides (HEOs), *Acta Mater.*, 2021, **202**, 181–189, DOI: **10.1016/j.actamat.2020.10.061**.

29 S. Jiang, T. Hu, J. Gild, N. Zhou, J. Nie, M. Qin, T. Harrington, K. Vecchio and J. Luo, A new class of high-entropy perovskite oxides, *Scr. Mater.*, 2018, **142**, 116–120, DOI: **10.1016/j.scriptamat.2017.08.040**.

30 R. Witte, A. Sarkar, R. Kruk, B. Eggert, R. A. Brand, H. Wende and H. Hahn, High-entropy oxides: An emerging prospect for magnetic rare-earth transition metal perovskites, *Phys. Rev. Mater.*, 2019, **3**(3), 034406, DOI: **10.1103/PhysRevMaterials.3.034406**.

31 Z. Teng, L. Zhu, Y. Tan, S. Zeng, Y. Xia, Y. Wang and H. Zhang, Synthesis and structures of high-entropy pyrochlore oxides, *J. Eur. Ceram. Soc.*, 2020, **40**(4), 639–1643, DOI: **10.1016/j.jeurceramsoc.2019.12.008**.

32 X. Ping, B. Meng, X. Yu, Z. Ma, Z. Pan and W. Lin, Structural, mechanical and thermal properties of cubic bixbyite-structured high-entropy oxides, *Chem. Eng. J.*, 2023, **464**, 142649, DOI: **10.1016/j.cej.2023.142649**.

33 J. Dąbrowa, J. Cieślak, M. Zajusz, M. Moździerz, K. Berent, A. Mikuła, A. Stępień and K. Świerczek, Structure and transport properties of the novel $(Dy,Er,Gd,Ho,Y)_3Fe_5O_{12}$ and $(Dy,Gd,Ho,Sm,Y)_3Fe_5O_{12}$ high entropy garnets, *J. Eur. Ceram. Soc.*, 2021, **41**(6), 3844–3849, DOI: **10.1016/j.jeurceramsoc.2020.12.052**.

34 M. Fracchia, P. Ghigna, T. Pozzi, U. Anselmi-Tamburini, V. Colombo, L. Braglia and P. Torelli, Stabilization by Configurational Entropy of the Cu(II) Active Site during CO Oxidation on $Mg_{0.2}Co_{0.2}Ni_{0.2}Cu_{0.2}Zn_{0.2}O$, *J. Phys. Chem. Lett.*, 2020, **11**(9), 3589–3593, DOI: **10.1021/acs.jpclett.0c00602**.

35 F. Tavani, M. Fracchia, A. Tofoni, L. Braglia, A. Jouve, S. Morandi, M. Manzoli, P. Torelli, P. Ghigna and

3418 | *Phys. Chem. Chem. Phys.*, 2025, **27**, 3412–3419

This journal is © the Owner Societies 2025

P. D'Angelo, Structural and mechanistic insights into low-Temperature CO oxidation over a prototypical high entropy oxide by Cu L-edge *operando* soft X-ray absorption spectroscopy, *Phys. Chem. Chem. Phys.*, 2021, **23**(46), 26575–26584, DOI: **10.1039/d1cp03946f**.

36 L. Kótai, V. M. Petruševski, L. Bereczki and K. A. Béres, Catalytic Properties of the Spinel-Like $Cu_xMn_{3-x}O_4$ Copper Manganese Oxides—An Overview, *Catalysts*, 2023, **13**, 129, DOI: **10.3390/catal13010129**.

37 S. Dey and N. S. Mehta, Selection of Manganese oxide catalysts for catalytic oxidation of Carbon monoxide at ambient conditions, *Resour. Environ. Sustain.*, 2020, **1**, 100003, DOI: **10.1016/j.resenv.2020.100003**.

38 H. Pan, X. Chen, C. López-Cartes, J. Martínez-López, E. Bu and J. J. Delgado, Hydrothermal synthesis and characterization of $Cu-MnO_x$ catalysts for CO oxidation: Effect of Cu:Mn molar ratio on their structure and catalytic activity, *Catal. Today*, 2023, **418**, 114085, DOI: **10.1016/j.cattod.2023.114085**.

39 S. Dey and G. C. Dhal, Catalytic Conversion of Carbon Monoxide into Carbon Dioxide over Spinel Catalysts: An Overview, *Mater. Sci. Energy Technol.*, 2019, **2**, 575–588, DOI: **10.1016/j.mset.2019.06.003**.

40 O. A. Bulavchenko, T. N. Afonasenko, S. S. Sigaeva, A. V. Ivanchikova, A. A. Saraev, E. Y. Gerasimov and S. V. Tsybulya, The Structure of Mixed Mn–Co Oxide Catalysts for CO Oxidation, *Top. Catal.*, 2020, **63**(1–2), 75–85, DOI: **10.1007/s11244-020-01230-1**.

41 C. Hudy, O. Długosz, J. Gryboś, J. Zasada, A. Krasowska, A. Janas and A. Sojka, Catalytic performance of mixed $M_xCo_{3-x}O_4$ (M = Cr, Fe, Mn, Ni, Cu, Zn) spinels obtained by combustion synthesis for preferential carbon monoxide oxidation (CO-PROX): insights into the factors controlling catalyst selectivity and activity, *Catal. Sci. Technol.*, 2022, **12**(8), 2446–2461, DOI: **10.1039/D2CY00388K**.

42 M. Al Samarai, A. W. Hahn, A. Beheshti Askari, Y.-T. Cui, K. Yamazoe, J. Miyawaki, Y. Harada, O. Rüdiger and S. DeBeer, Elucidation of Structure-Activity Correlations in a Nickel Manganese Oxide Oxygen Evolution Reaction Catalyst by *Operando* Ni L-Edge X-ray Absorption Spectroscopy and 2p3d Resonant Inelastic X-ray Scattering, *ACS Appl. Mater. Interfaces*, 2019, **11**(42), 38595–38605, DOI: **10.1021/acsami.9b06752**.

43 K. Wiese, A. M. Abdel-Mageed, A. Klyushin and R. J. Behm, Dynamic changes of Au/ZnO catalysts during methanol synthesis: A model study by temporal analysis of products (TAP) and Zn L_{III} near Edge X-Ray absorption spectroscopy, *Catal. Today*, 2019, **336**, 193–202, DOI: **10.1016/j.cattod.2018.11.074**.

44 L. Braglia, M. Fracchia, P. Ghigna, A. Minguzzi, D. Meroni, R. Edla, M. Vandichel, E. Ahlberg, G. Cerrato and P. Torelli, Understanding Solid-Gas Reaction Mechanisms by *Operando* Soft X-Ray Absorption Spectroscopy at Ambient Pressure, *J. Phys. Chem. C*, 2020, **124**(26), 14202–14212, DOI: **10.1021/acs.jpcc.0c02546**.

45 H. Ikeno, F. M. F. De Groot, E. Stavitski, I. Tanaka and I. Multiplet, calculations of $L_{2,3}$ X-ray absorption near-edge structures for 3d transition-metal compounds, *J. Phys.: Condens. Matter*, 2009, **21**(10), 104208, DOI: **10.1088/0953-8984/21/10/104208**.

46 R. Edla, L. Braglia, V. Bonanni, A. Miotello, G. Rossi and P. Torelli, Study of Gaseous Interactions on Co_3O_4 Thin Film Coatings by Ambient Pressure Soft X-ray Absorption Spectroscopy, *J. Phys. Chem. C*, 2019, **23**(40), 24511–24519, DOI: **10.1021/acs.jpcc.9b05433**.

47 B. Ravel and M. Newville, ATHENA, ARTEMIS, HEPHAESTUS: data analysis for X-ray absorption spectroscopy using IFEFFIT, *J. Synchrotron Radiat.*, 2005, **12**, 537–541, DOI: **10.1107/S0909049505012719**.

This journal is © the Owner Societies 2025

Phys. Chem. Chem. Phys., 2025, **27**, 3412–3419 | **3419**